IEEE Photonics Journal
An IEEE Photonics Society Publication

Open Access

Dual-Band (O & C-Bands) Two-Mode Multiplexer on the SOI Platform

Volume 13, Number 3, June 2021

Bruna Paredes
Zakriya Mohammed, ***Student Member, IEEE***
Juan Villegas, ***Student Member, IEEE***
Mahmoud Rasras, ***Senior Member, IEEE***

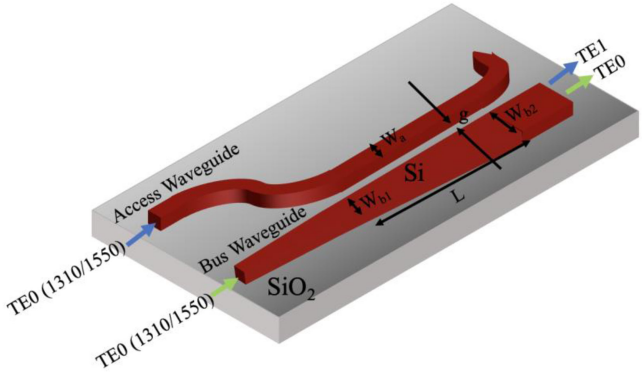

DOI: 10.1109/JPHOT.2021.3075292

IEEE photonics SOCIETY

IEEE

Dual-Band (O & C-Bands) Two-Mode Multiplexer on the SOI Platform

Bruna Paredes,[1] **Zakriya Mohammed**,[2] ***Student Member, IEEE***,
Juan Villegas,[2] ***Student Member, IEEE***,
and Mahmoud Rasras,[1] ***Senior Member, IEEE***

[1]Electrical and Computer Engineering, New York University, 129188, UAE
[2]Electrical and Computer Engineering, New York University- Tandon School of Engineering, Brooklyn, NY 11201 USA

DOI:10.1109/JPHOT.2021.3075292

Manuscript received March 15, 2021; revised April 16, 2021; accepted April 20, 2021. Date of publication April 23, 2021; date of current version May 10, 2021. This work was supported by NYUAD Center for Cyber Security. *(Bruna Paredes and Zakriya Mohammed contributed equally to this work.)*
Corresponding author: Bruna Paredes (e-mail: bp64@nyu.edu).

Abstract: We demonstrate a dual-band two-mode (de)-multiplexer based on tapered asymmetric directional coupler (ADC). The working principle of the device relies on the conversion of the fundamental transverse electric (TE0) mode to the first order (TE1) mode. A phase-matching condition is applied across the O- and C-bands to broaden the operation wavelength of the device. Measurement performed on a mode division multiplexing (MDM) link formed by a back-to-back connected multiplexer and demultiplexer exhibited an insertion loss of less than 1.2 dB with cross talk better than 16 dB. The response is recorded over dual-bands, each with 100-nm bandwidth covering 1260-1360 nm and 1500–1600 nm (extends to the near L-band). The device is compact with an overall length of 75 μm.

Index Terms: Photonic integrated circuits, silicon photonics, optical devices, mode multiplexers, asymmetric directional couplers.

1. Introduction

Silicon photonics (SiPh), which features CMOS (complementary metal-oxide-semiconductor) compatibility, enables technology in critical areas such as optical interconnects for data centers [1]. Although some bottlenecks related to thermal sensitivity and birefringence in the SiPh platform can hinder the usage, these problems are actively being solved [2]–[4]. In comparison to traditional copper interconnects, optical ones have the advantage of broad bandwidth. Multiplexing schemes such as wavelength- and polarization-division multiplexing have been implemented extensively for increasing the transmission capacity of an optical link [5], [6]. To further enhance the link capacity, recently, mode division multiplexing (MDM) has attracted growing attention. In this scheme, higher-order optical modes of the same propagating wavelength are excited such that each mode carries an independent signal channel [7], [8], where an efficient mode multiplexer constitutes a fundamental enabling building block.

The MDM multiplexers reported in the Silicon on Insulator (SOI) platform use a wide variety of approaches, such as asymmetric Y-junctions [9], [10], asymmetric directional couplers (ADC) [11], [12], multimode interference (MMI) couplers [13], inverse design [14], [15], Bragg gratings[16] and adiabatic couplers [17]–[21]. In an asymmetric Y-junction, it is not easy in practice to achieve a low-loss junction due to corner effects. Alternatively, the MMI-based MDM may have high fabrication

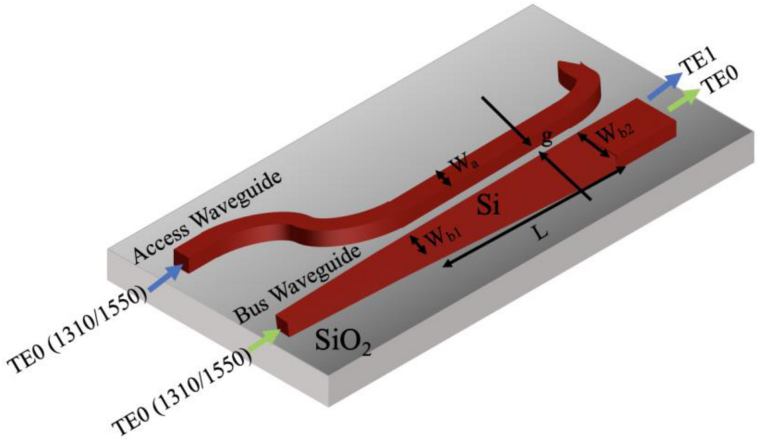

Fig. 1. A schematic of the proposed mode multiplexer.

tolerance. However, its structure is relatively complex, consisting of several MMI stages and phase shifters [22]–[24]. On the other hand, adiabatic couplers exhibit high wavelength independence due to the broadband properties of their mode evolution. Nevertheless, to ensure adiabatic evolution of the local modes, the coupler's length has to be sufficiently long, resulting in a large device footprint. Furthermore, such couplers cannot conveniently accommodate more than two modes [21]–[23].

The ADC-based MDMs take advantage of the phase-matching condition, and their coupling length is usually short. Furthermore, they can easily be expanded to accommodate multiple higher-order modes and to be combined with other multiplexing schemes [8]. The main drawback with ADC is usually the sensitivity of its performance to process variations. Also, the operation wavelength (optical bandwidth) of an ADC is typically limited to a few tens of nanometers. Recently, several fabrication-tolerant ADC-based MDMs have been proposed. The fabrication tolerance is enhanced by using either tapered or taper-etched directional couplers [11]–[12]. One can also use the "shortcuts to adiabaticity (STA)" calculation method to reduce fabrication sensitivity [25]. However, most of the reported multiplexers are still limited in their operation to only the C-band. Therefore, it is of interest to develop ADC-based multiplexers with a broader wavelength operation range.

In this work, we demonstrate a mode multiplexer with good working performance in both C- and O-bands, which can be beneficial to improving the capacity of multimode type interconnects. The design is based on the ADC scheme and employs an adiabatic taper approach to extend the bandwidth to the O-band. The device is 75 μm long and requires only a single etch step for fabrication.

2. Design Methodology

A schematic of the proposed two-mode multiplexer is shown in Fig. 1. The device consists of a single-mode access waveguide (width W_a), and an adiabatically tapered multimode bus waveguide (Wb_1 to Wb_2) separated by a gap (g) and has a coupling length of L. The operating principle of the proposed two-mode multiplexer is as follows: When a TE0 mode is coupled to the bus waveguide, it will be preserved and immerge after the coupling regions as TE0. The bus waveguide starts with a 500 nm single-mode width, and it is transitioned first adiabatically to a width Wb_1 using a 5 μm taper. Then from Wb_1 to Wb_2, another adiabatic taper is used, which preserves the fundamental mode. On the other hand, when a TE0 mode is injected into the access waveguide, it couples to the tapered bus waveguide as a TE1 due to phase-matching condition.

For a conventional ADC multiplexer, coupling relies on the phase-matching condition between its propagating modes, i.e., the effective refractive index of the TE0 mode in the access waveguide should be equal to that of the TE1 mode of the bus waveguide. In this case, if a TE0 mode is coupled into the narrower access waveguide, a high coupling efficiency from TE0 to TE1 mode

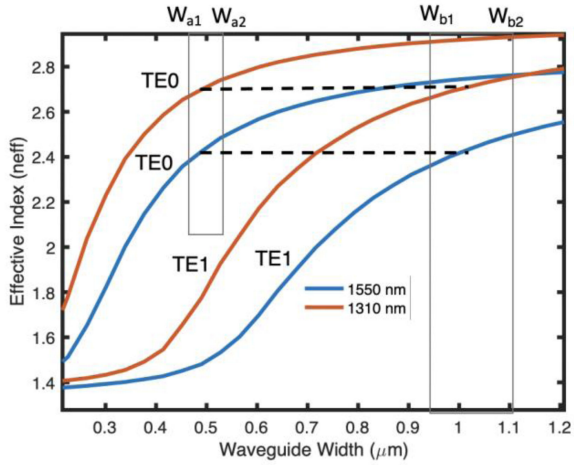

Fig. 2. Effective indices of the TE0, TE1 of an oxide cladded SOI waveguide as a function of its width (w) for a waveguide height of 220 nm. The simulation is performed at 1550 nm and 1310 nm wavelengths.

($K_{\mathrm{TE0\text{-}TE1}}$) will be obtained at the output of the bus waveguide. On the other hand, because of the significant difference between the effective refractive indices of the TE0 modes in the access and bus waveguides, a very low coupling efficiency $K_{\mathrm{TE0\text{-}TE0}}$ (mode crosstalk) is expected.

In conventional asymmetrical directional couplers (DCs), the phase-matching condition can be easily disrupted by fabrication variations in the access waveguide. A slight variation of width (Δw) in the access waveguide can result in a considerable effective refractive index (Δn_{eff}) change. This is evident since the slope of the effective index versus waveguide width is larger for the TE0 mode compared to the TE1 mode, see Fig. 2. The larger the slope difference, the easier it is to disrupt the phase-matching condition. Similarly, the bandwidth (operation wavelength) will be limited as the phase matching condition can only be satisfied for a narrow band. Also, the length of DC needs to be properly designed to prevent coupling of the converted TE1 light back to the narrower waveguide.

To relax these fabrication and bandwidth requirements, tapered ADCs are reported [11], [12]. In tapered ADCs, the bus waveguide is tapered resulting in a window of tolerance to any deviations in the access waveguide width. This is attributed to the fact that a phase-matching position can always be established along the tapered bus waveguide. Following the phase-matched location in the coupling region, the conversion efficiency will be maintained, and the sensitivity to the coupling length will be relaxed. Consequently, tapering the wider bus waveguide will result in increasing the wavelength window for which the phase-matching condition is satisfied. Additionally, a considerable tapering strength provides more fabrication tolerance to the access waveguide width variations. However, a stronger tapering of the bus waveguide requires a longer taper length L to allow sufficient coupling around the phase-matching position. In previously reported fabrication tolerant ADCs, the width selection, and tapering are designed for 1550 nm wavelength [8], [9]. This resulted in a performance limited to the C-band.

In this work, the width selection and tapering are performed to simultaneously satisfy the phase-matching condition for the 1550 nm and 1310 nm wavelengths. Thus, it results in a bandwidth extension to the O-band while maintaining fabrication tolerance. The design was optimized using the eigenmode expansion (EME) method. For ease of fabrication, the two-mode (de) multiplexer was designed on an SOI wafer with a silicon core thickness of $H = 220$ nm. In our proposed design, the bus waveguide is tapered from Wb_1 to Wb_2, resulting in tolerance to any deviations in the width of the access waveguide from Wa_1 to Wa_2 (see Fig. 2). For a single-mode access waveguide, a width of $Wa = 500$ nm was chosen as a starting point. From the phase matching curve, shown in Fig. 2, the corresponding width of the bus waveguide in the center of the coupling region is 1025 nm. Thus, the bus waveguide is tapered from $Wb_1 = 950$ nm to $Wb_2 = 1100$ nm. The $\pm$

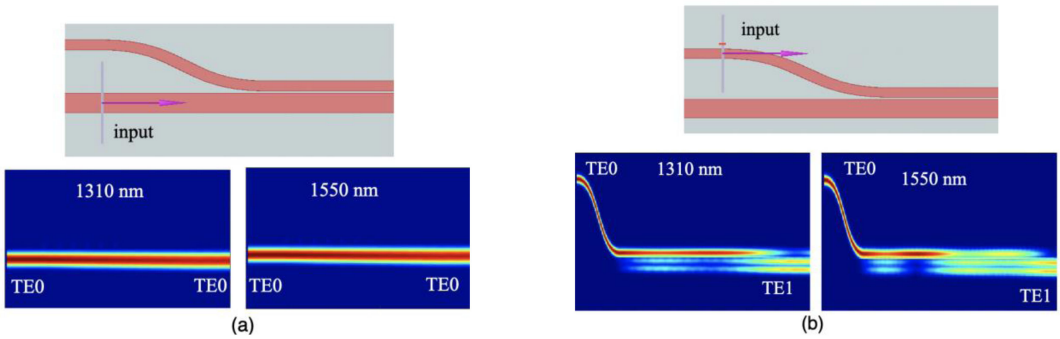

Fig. 3. (a) Light propagation of TE0 in the bus waveguide. (b) Light propagation of TE0 in the access waveguide.

75 nm width variation around 1025 nm is chosen such that the directional coupler has a broadband response to both O-and C- bands. The resulted coupling length is L $= 70$ μm.

3. Device Performance Analysis

For a gap (g) $=$ 100 nm and a coupling length (L) $= 70$ μm, the device performance is evaluated using 3D finite-difference time-domain (FDTD) method. Fig. 3 shows the light propagation when the TE0 modes are coupled into the access and bus waveguides. As shown in Fig. 3(a), light injected in the bus waveguide as TE0 keeps propagating as TE0 throughout (for 1310 nm left and 1550nm right). Besides, when the TE0 mode is injected in the access waveguide, it couples to a TE1 mode in the bus waveguide (Fig. 3(b) shown for 1310 nm left and 1550 nm right). For illustration purposes, Fig. 4 shows the corresponding transmission spectra of the access waveguide simulated over the O- and the C-bands. In Fig. 4, the light is injected as TE0 only in the access waveguide in order to study coupling efficiency and modal crosstalk. Due to our proposed design, all the input TE0 power should be coupled as TE1 at the output of the bus waveguide. However, there will be some TE0 power which couples as TE0 in the bus waveguide (modal cross talk). One can observe a high coupling efficiency from TE0 to TE1 (red curve) as required. The modal crosstalk (TE0 to TE0 blue curves) is better than 30 dB over an extensive wavelength range of 100 nm in each band (O and C), and partially covering the L-band. Additionally, from simulations, the insertion loss of the access waveguide is less than 0.1 dB and 0.5 dB, for 1550 nm and 1310 nm, respectively. The higher insertion loss for the O-band can be attributed to the higher confinement (lower coupling efficiency) of the silicon waveguide for this shorter wavelength band.

To estimate the fabrication tolerance of the (de)-multiplexer, we studied the TE0-TE1 conversion loss dependence on fabrication deviations for the following parameters: waveguide width and coupling gap. To study the effect of fabrication variability, the widths of both access ($W_a \pm \Delta W$) and bus waveguides are changed ($W_b \pm \Delta W$), where ΔW is the width deviation due to fabrication error. The simulations are performed assuming a process deviation of $\pm$ 10 nm. Fig. 5 shows the calculated coupling efficiency $K_{TE0\text{-}TE1}$ as a function of the width deviation (ΔW). Here we have considered a constant center-to-center distance between the access and bus waveguides. Therefore, the gap (g) between the two waveguides changes accordingly with changes in the waveguide widths. From this figure, it is found that the 1310 nm wavelength is more susceptible to variations in fabrication. However, the TE0-TE1 conversion loss is still less than 0.7 dB.

4. Fabrication and Characterization

The proposed two-mode multiplexer was fabricated using electron-beam lithography with plasma etching at Applied Nanotools (Canada). The fabrication is based on direct-write 100 keV electron

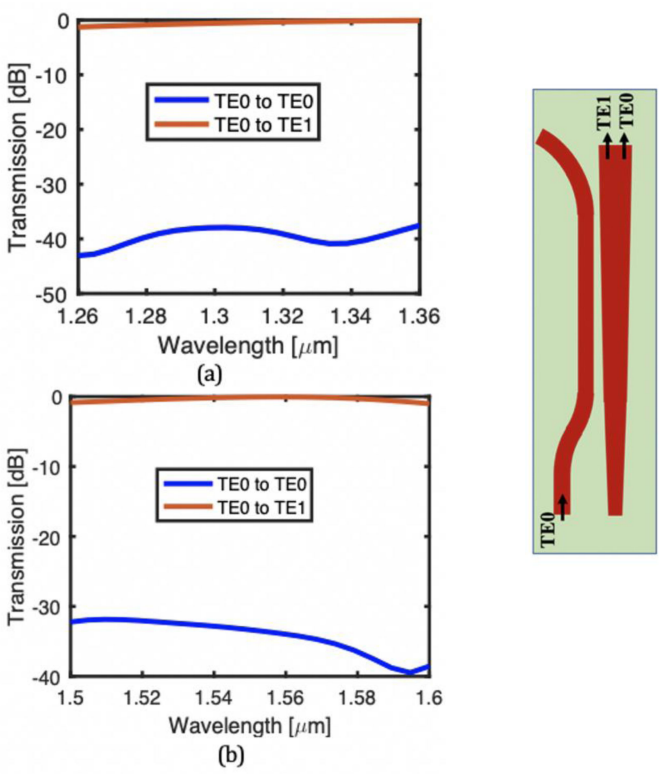

Fig. 4. Calculated wavelength dependency of TE0-TE1 coupling efficiency and modal crosstalk (TE0-TE0) for the multiplexer design in the wavelength range of (a) 1260-1360 nm (b) 1500-1600 nm.

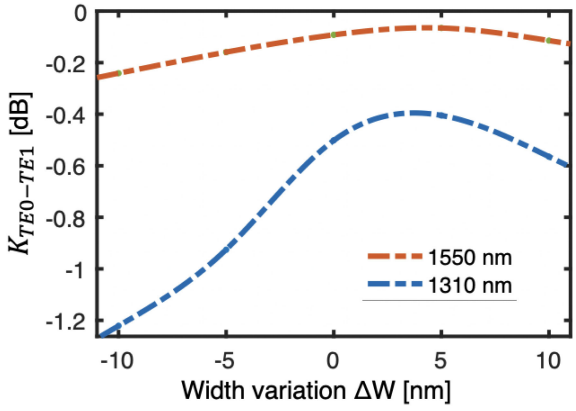

Fig. 5. Simulated coupling efficiency $K_{TE0\text{-}TE1}$ as a function of width deviation (ΔW).

beam lithography technology on SOI wafers with a 220 nm thick silicon layer. A 2.2 μm oxide cladding was deposited using a plasma-enhanced chemical vapor deposition (PECVD) process. Scanning electron microscope (SEM) images of the fabricated device are shown in Fig. 6. The fabricated mode division multiplexing (MDM) circuit consists of a back-to-back multiplexer and demultiplexer connected by a multimode transmission bus waveguide. The multiplexer and de-multiplexer share identical design parameters according to the reciprocity theorem [14]. As shown in this figure, the device has two inputs I_1 and I_2, and the two outputs are designated as O_1 and O_2.

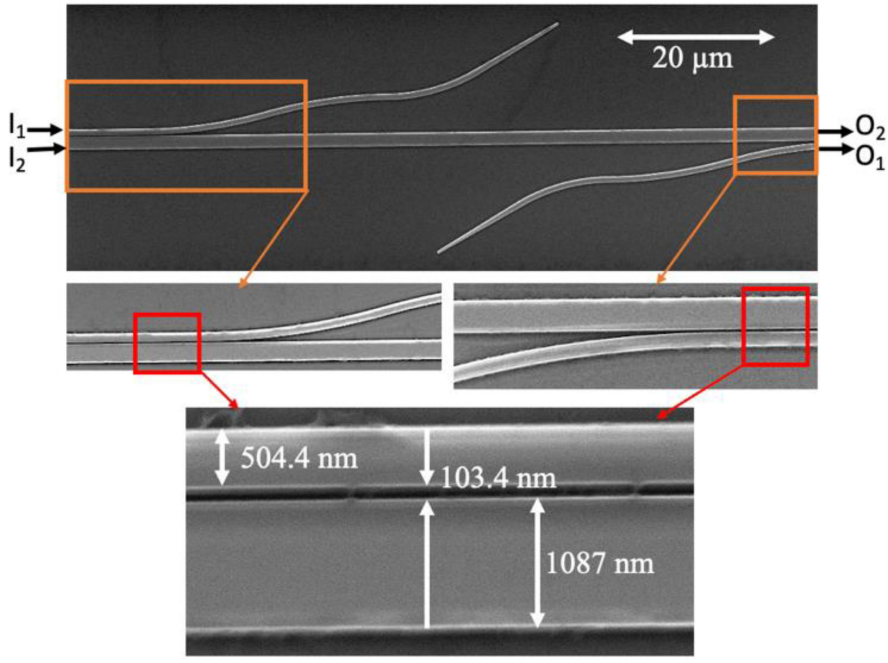

Fig. 6. SEM images of the fabricated device.

To test the device, a signal in the TE0 mode (ch_1) is coupled to input I_1, then routed through the first ADC to the bus waveguide as TE1. Consequently, this channel is converted back to TE0 through the second ADC and routed to output O_1. Additionally, a second signal channel (ch_2) is inserted into the input I_2 as TE0, which propagates through the device's first and second ADCs, it remains in the TE0 mode. This signal is measured at output O_2. Therefore, the path I_1-O_1 allows measuring ch_1 [(TE0 to TE1) -(TE1 to TE0)] insertion loss (IL) while the path I_2-O_2 is used to measure ch_2 [(TE0 to TE0) - (TE0 to TE0)] insertion loss. The corresponding crosstalk is measured at inputs/outputs I_1-O_2 and I_2-O_1 for ch_1 and ch_2 inputs, respectively.

Our circuit is characterized using fiber butt-coupling. The SiPh chip is mounted on a stage with a temperature controller. Two tunable Keysight 81600B laser sources (C-band and O-band lasers) and Keysight N7744A optical detector sensors are used to measure the device wavelength response. A polarization controller adjusts the light polarization of the tunable laser source and then couples it to the SiPh chip using an array of SMF-28 fibers with 127 μm pitch. Before measuring the devices, the external polarizer ensures a TE0 polarization is excited with an extinction ratio of 20 dB relative to the zero-order transverse magnetic (TM0) mode.

Fig. 7 shows the normalized transmission characteristics of our two-mode MDM link. The results demonstrate the combined responses of the MDM multiplexer and-demultiplexer. For the wavelength range of 1260 nm to 1360 nm, the measured IL and the crosstalk are lower than 1.2 dB and 17.0 dB, respectively. Additionally, for the wavelength range of 1500 nm to 1600 nm, the measured IL and crosstalk are better than 0.8 dB and 16.0 dB, respectively. Therefore, for both 1310 nm and 1550 nm bands, our fabricated MDM link achieves measured crosstalk lower than 16 dB over the 100 nm bandwidth in the O-band and 100 nm bandwidth in the C- and near L-bands.

This result is in good agreement with the simulation. However, the discrepancy in insertion loss and crosstalk can be attributed to the limited polarization extinction ratio of the input fiber and waveguide propagation losses. The latter introduces an additional insertion loss to the measurements, which can be improved by optimizing the fabrication process and reducing the sidewall roughness. Also, edge coupling may induce some Fabry-Perot reflection at the facet between the fiber and waveguide and cause some other unwanted input polarization, which will lead to relatively higher

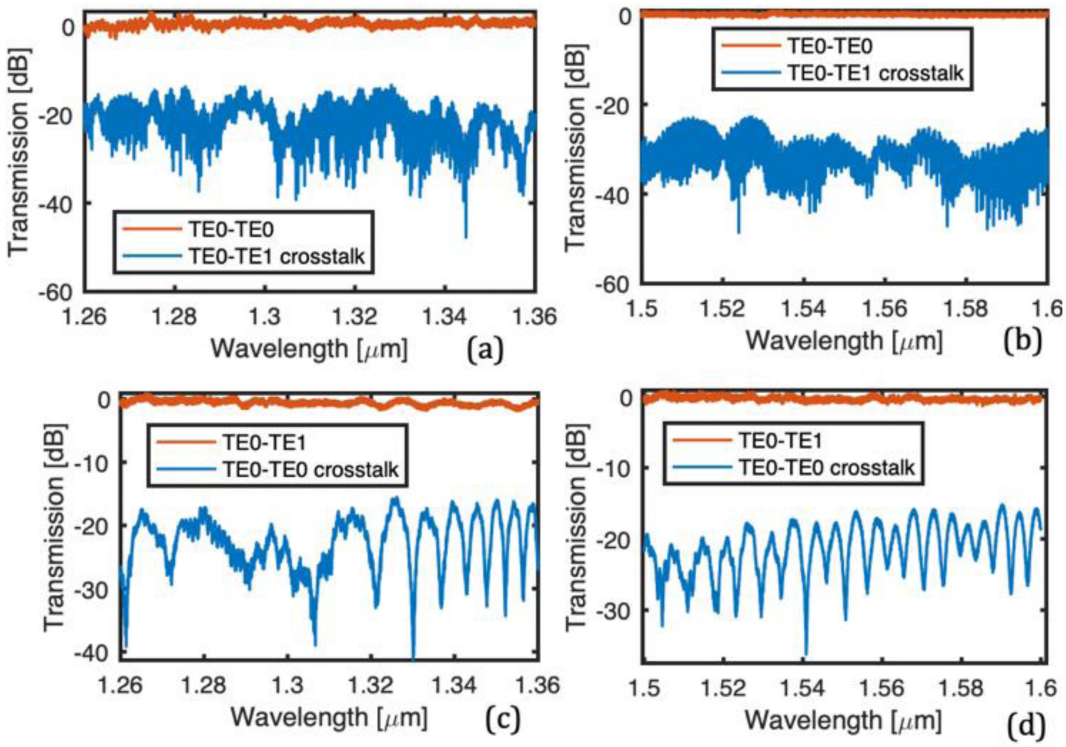

Fig. 7. (a-b) Transmission spectra of TE0-TE0 through insertion loss [I_2O_2] and modal cross talk TE0-TE1 [I_2O_1]. (c-d) TE0-TE1 mode conversion loss [I_1O_1] and modal cross talk. TE0-TE0 [I_1O_2].

TABLE 1
Performance Comparison with the Literature

Ref	**Type**	**Length** (μm)	**Bandwidth** (nm)	**Crosstalk** (dB)	**IL** (dB)
[9]	Y-junction	N/A	1520-1620	<9	<1.5
[10]	Y-junction	60	1513-1619	<9.1	<0.56
[11]	ADC	>50	1480-1580	< 16	>0.3
[12]	ADC	>68	1525-1590	< 26	<1.6
[13]	MMI	N/A	1525-1565	< 13.7	N/A
[14]	Inverse Design	4.22	1520-1620	< 12	<2.4
[17]	Adiabatic	260	1460-1640	< 13	<1
[19]	Adiabatic	181	1510-1600	< 19	<1.5
This work	ADC	75	1260-1360 1500-1600	<16	<1.2

crosstalk. A potential solution is to use a vertical grating coupling scheme. The grating coupler can work as a polarization filter which can improve the crosstalk performance. Furthermore, to improve the crosstalk performance, the tapered DC structure in the design can be replaced with a taper-etched DC to compensate for fabrication inaccuracies [12].

Table 1 compares our device performance to previously reported results in the literature for similar two-mode multiplexers fabricated on the SOI platform. As shown in this table, most reported

devices have a bandwidth working only in the C-band. In comparison, our device can operate in both the O-& C-bands and uses a simple ADC design based on a conventional strip waveguide. An additional characteristic of our demonstrated device is that it is significantly smaller than other reported adiabatic mode multiplexers and slightly larger than other ADCs. The device length of the proposed structure can be further reduced by using partial etch ridge waveguides and following the tapering procedure. In a low etch depth ridge waveguide, the coupling strength between the waveguides is enhanced [26]. The strong coupling is a result of larger transverse mode field diameters, thus stronger mode overlap. However, ridge waveguides require two steps etching which increases fabrication cost and process complexity.

5. Conclusion

In summary, we have experimentally demonstrated a compact, low crosstalk dual-band on-chip mode division (de) multiplexer on an SOI platform. The device features a tapered structure which increases the wavelength operation bandwidth. The device is fabricated on a 220 nm SOI platform with a compact footprint of 75 μm. The measurement results of a back-to-back multiplexer/demultiplexer MDM link demonstrated an insertion loss of less than 1.2 dB with crosstalk better than 16 dB in the wavelength ranges of 1260–1360 nm and 1500–1600 nm. The proposed MDM can be potentially integrated with other multiplexing schemes like WDM and polarization-division multiplexing (PDM) to further increase the on-chip link transmission capacity [8]. Also, the demonstrated operation in both the O-and C-bands makes the reported device a promising candidate for on-chip MDM systems.

Acknowledgment

The authors would like to thank NYUAD Photonics Lab and the Core Technology Platform Facility (CTP) for the analytical and material characterization. They also thank Nikolas Giakoumidis for the technical support and Tadesse Mulugeta for the useful discussion. Simulations for this research were partially carried out on the High-Performance Computing resources at NYUAD.

References

[1] Y. Shen *et al.*, "Deep learning with coherent nanophotonic circuits," *Nature Photon.*, vol. 11, no. 7, pp. 441–446, Jul. 2017, doi: 10.1038/nphoton.2017.93.
[2] Z. Mohammed, B. Paredes, and M. Rasras, "Effect of process parameters on mode conversion in submicron tapered silicon ridge waveguides," *Appl. Sci.*, vol. 11, no. 5, Jan. 2021, doi: 10.3390/app11052366.
[3] Z. Mohammed, B. Paredes, and M. Rasras, "A polarization insensitive athermal design for mach-zehnder interferometer," in *Proc. Conf. Lasers Electro-Opt. Pacific Rim*, Aug. 2020, pp. 1–2, doi: 10.1364/CLEOPR.2020.C12H_2.
[4] Z. Mohammed, B. Paredes, and M. Rasras, "Athermal mach-zehnder interferometer with heterogeneous cladding for bio-sensing," in *Proc. IEEE Photon. Conf.*, Sep. 2020, pp. 1–2, doi: 10.1109/IPC47351.2020.9252448.
[5] H. Fukuda, K. Yamada, T. Tsuchizawa, T. Watanabe, H. Shinojima, and S. Itabashi, "Silicon photonic circuit with polarization diversity," *Opt. Exp.*, vol. 16, no. 7, pp. 4872–4880, Mar. 2008, doi: 10.1364/OE.16.004872.
[6] A. Liu *et al.*, "Wavelength division multiplexing based photonic integrated circuits on Silicon-on-Insulator platform," *IEEE J. Sel. Topics Quantum Electron.*, vol. 16, no. 1, pp. 23–32, Jan. 2010, doi: 10.1109/JSTQE.2009.2033454.
[7] C. Li, D. Liu, and D. Dai, "Multimode silicon photonics," *Nanophotonics*, vol. 8, no. 2, pp. 227–247, Feb. 2019, doi: 10.1515/nanoph-2018-0161.
[8] T. Mulugeta, and M. Rasras, "Silicon hybrid (de)multiplexer enabling simultaneous mode and wavelength-division multiplexing," *Opt. Exp.*, vol. 23, no. 2, pp. 943–949, Jan. 2015, doi: 10.1364/OE.23.000943.
[9] J. B. Driscoll, R. R. Grote, B. Souhan, J. I. Dadap, M. Lu, and R. M. Osgood, "Asymmetric Y junctions in silicon waveguides for on-chip mode-division multiplexing," *Opt. Lett.*, vol. 38, no. 11, pp. 1854–1856, Jun. 2013, doi: 10.1364/OL.38.001854.
[10] H. Li *et al.*, "Experimental demonstration of a broadband two-mode multi/demultiplexer based on asymmetric Y-junctions," *Opt. Laser Technol.*, vol. 100, pp. 7–11, Mar. 2018, doi: 10.1016/j.optlastec.2017.09.043.
[11] Y. Ding, J. Xu, F. D. Ros, B. Huang, H. Ou, and C. Peucheret, "On-chip two-mode division multiplexing using tapered directional coupler-based mode multiplexer and demultiplexer," *Opt. Exp.*, vol. 21, no. 8, pp. 10376–10382, Apr. 2013, doi: 10.1364/OE.21.010376.
[12] Y. Sun, Y. Xiong, and W. N. Ye, "Experimental demonstration of a two-mode (de)multiplexer based on a taper-etched directional coupler," *Opt. Lett.,* vol. 41, no. 16, pp. 3743–3746, Aug. 2016, doi: 10.1364/OL.41.003743.

[13] H. Xiao *et al.*, "On-chip reconfigurable and scalable optical mode multiplexer/demultiplexer based on three-waveguide-coupling structure," *Opt. Exp.*, vol. 26, no. 17, pp. 22366–22377, Aug. 2018, doi: 10.1364/OE.26.022366.
[14] L. F. Frellsen, Y. Ding, O. Sigmund, and L. H. Frandsen, "Topology optimized mode multiplexing in silicon-on-insulator photonic wire waveguides," *Opt. Exp.*, vol. 24, no. 15, pp. 16866–16873, Jul. 2016, doi: 10.1364/OE.24.016866.
[15] W. Chang *et al.*, "Ultra-compact mode (de) multiplexer based on subwavelength asymmetric Y-junction," *Opt. Exp.*, vol. 26, no. 7, pp. 8162–8170, Apr. 2018, doi: 10.1364/OE.26.008162.
[16] H. Qiu *et al.*, "Silicon mode multi/demultiplexer based on multimode grating-assisted couplers," *Opt. Exp.*, vol. 21, no. 15, pp. 17904–17911, Jul. 2013, doi: 10.1364/OE.21.017904.
[17] J. Xing, Z. Li, X. Xiao, J. Yu, and Y. Yu, "Two-mode multiplexer and demultiplexer based on adiabatic couplers," *Opt. Lett.,* vol. 38, no. 17, pp. 3468–3470, Sep. 2013, doi: 10.1364/OL.38.003468.
[18] J. Wang *et al.*, "Broadband and fabrication-tolerant on-chip scalable mode-division multiplexing based on mode-evolution counter-tapered couplers," *Opt. Lett.,* vol. 40, no. 9, pp. 1956–1959, May 2015, doi: 10.1364/OL.40.001956.
[19] C. Sun, Y. Yu, M. Ye, G. Chen, and X. Zhang, "An ultra-low crosstalk and broadband two-mode (de)multiplexer based on adiabatic couplers," *Sci. Rep.*, vol. 6, no. 1, Dec. 2016, doi: 10.1038/srep38494.
[20] Z. Zhang, Y. Yu, and S. Fu, "Broadband on-chip mode-division multiplexer based on adiabatic couplers and symmetric Y-Junction," *IEEE Photon. J.*, vol. 9, no. 2, pp. 1–6, Apr. 2017, doi: 10.1109/JPHOT.2017.2669527.
[21] D. Guo, and T. Chu, "Silicon mode (de)multiplexers with parameters optimized using shortcuts to adiabaticity," *Opt. Exp.*, vol. 25, no. 8, pp. 9160–9170, Apr. 2017, doi: 10.1364/OE.25.009160.
[22] M. Ye, Y. Yu, J. Zou, W. Yang, and X. Zhang, "On-chip multiplexing conversion between wavelength division multiplexing-polarization division multiplexing and wavelength division multiplexing-mode division multiplexing," *Opt. Lett.,* vol. 39, no. 4, pp. 758–761, Feb. 2014, doi: 10.1364/OL.39.000758.
[23] T. Uematsu, Y. Ishizaka, Y. Kawaguchi, K. Saitoh, and M. Koshiba, "Design of a compact two-mode multi/demultiplexer consisting of multimode interference waveguides and a wavelength-insensitive phase shifter for mode-division multiplexing transmission," *J. Lightw. Technol.*, vol. 30, no. 15, pp. 2421–2426, Aug. 2012, doi: 10.1109/JLT.2012.2199961.
[24] Y. Li, C. Li, C. Li, B. Cheng, and C. Xue, "Compact two-mode (de)multiplexer based on symmetric Y-junction and multimode interference waveguides," *Opt. Exp.*, vol. 22, no. 5, pp. 5781–5786, Mar. 2014, doi: 10.1364/OE.22.005781.
[25] T.-H. Pan, and S.-Y. Tseng, "Short and robust silicon mode (de)multiplexers using shortcuts to adiabaticity," *Opt. Exp.*, vol. 23, no. 8, pp. 10405–10412, Apr. 2015, doi: 10.1364/OE.23.010405.
[26] A. Melikyan, and P. Dong, "Adiabatic mode converters for silicon photonics: Power and polarization broadband manipulators," *APL Photon.*, vol. 4, no. 3, p. 030803, Mar. 2019, doi: 10.1063/1.5080247.